Real-time metabolic heat-based specific growth rate soft sensor for monitoring and control of high molecular weight HA production by Streptococcus zooepidemicus.

Naresh Mohan
Indian Institute of Technology Guwahati
Satya Sai Pavan
Indian Institute of Technology Guwahati
Anjali Jayakumar
Indian Institute of Technology Guwahati
Sivakumar Rathinavelu
Indian Institute of Technology Guwahati
Senthilkumar Sivaprakasam (senthilkumar@iitg.ac.in)
Indian Institute of Technology Guwahati Department of Biosciences and Bioengineering
https://orcid.org/0000-0001-6064-9061

Research

Keywords: Calorimetry, Specific growth rate estimator, PID control, S. zooepidemicus, Hyaluronic acid

Posted Date: December 11th, 2020

DOI: https://doi.org/10.21203/rs.3.rs-60135/v2

Research

Real-time metabolic heat-based specific growth rate soft sensor for monitoring and control of high molecular weight HA production by *Streptococcus zooepidemicus*.

Naresh Mohan[1,#], Satya Sai Pavan[1,#] Anjali Jayakumar[1], Sivakumar Rathinavelu[1], Senthilkumar Sivaprakasam[*,1]

Authors' official mail

Naresh Mohan – l.naresh@iitg.ernet.in

Satya Sai Pavan – pavan176106014@iitg.ac.in

Anjali Jayakumar – j.anjali@iitg.ac.in

Sivakumar Rathinavelu – r.sivakumar@iitg.ac.in

Senthilkumar Sivaprakasam – senthilkumar@iitg.ernet.in

[1]BioPAT Laboratory, Department of Biosciences & Bioengineering, Indian Institute of Technology Guwahati, Guwahati-781039, Assam, India.

# Equally contributed.

***Correspondence:**

Dr. Senthilkumar Sivaprakasam,

Associate Professor,

Department of Biosciences and Bioengineering,

Indian Institute of Technology Guwahati,

Guwahati – 781039, Assam.

Tel: +91 361 2582226.

Fax: +91 361 2582249

Abstract

Background: Hyaluronic acid (HA) is an important mucopolysaccharide of higher molecular weight range and holds sheer economic interest. Its applications are widely acknowledged in rheumatoid arthritis treatment, tissue engineering, and cosmetics industries. This present investigation aims for the fed-batch production of high molecular weight range HA by application of real-time metabolic heat measurements.

Results: Fed-batch strategies based on Feedforward (FF) and Feedback (FB) control was devised to improve the Molecular Weight (MW) of HA production by *S. zooepidemicus*. Metabolic heat measurements (Fermentation calorimetry) were modeled to decipher real-time specific growth rate, μ_{est} was looped to the PID circuit, envisaged to control μ_{SP} to their desired setpoint values 0.05 h^{-1}, 0.1 h^{-1} and 0.15 h^{-1} respectively. The developed FB strategy established a robust control on maintaining the specific growth rate (μ) close to the μ_{SP} value with a minimal tracking error. Exponential feed rate carried out with a lowest μ_{SP} of 0.05 h^{-1} improved the MW of HA significantly to 2.98 MDa and 2.94 MDa for the FF and FB based control strategies respectively. An optimal HA titer of 4.73 g/L was achieved in a FF control strategy at $\mu_{SP} =$ 0.15 h^{-1}. Biomass and Lactic acid (LA) concentrations were found to be concomitant with the increase in μ_{SP} from 0.05 h^{-1} to 0.15 h^{-1}. Superior control of μ at low μ_{SP} value was observed to influence positively the HA polymerization attributing to improved MW and desired Polydispersity Index (PDI) of HA.

Conclusions: This present investigation attempts to address the metabolic bottleneck in synthesis of high MW HA by *S. zooepidemicus* and illustrates the application of calorimetric fed-

batch control of μ at a narrower range. PID control offers advantage over conventional fed-batch method to synthesize HA at an improved MW. Calorimetric signal based μ control by PID negates adverse effects due to the secretion of other end products albeit maintaining homeostasis.

Keywords Calorimetry, Specific growth rate estimator, PID control, *S. zooepidemicus*, Hyaluronic acid

Background

Research in the biosynthesis of Glycosaminoglycan (GAG) is recently gaining attention to understand the role of structural glycan moieties in mediating the interaction between signaling molecules to the cell surface receptors for various non-immunogenic activities [1]. Hyaluronic acid (HA) is a special non-proteoglycan and non-sulphated GAG polymer possess multitude of applications such as mediating angiogenesis, as a gelling agent for biomaterial application, tissue regeneration [2,3], cosmetics, food supplements [4,5] etc and remains to be the most studied glycan polymer. It is a linear biopolymer composed of alternating N-acetyl-D-glucosamine and D-glucuronic acid monomers covalently linked by β(1-4) and β(1-3) bonds respectively spanning molecular weights ranging from 5 kDa [6] to 5.9 MDa [7]. Its commercial vitality can be appreciated from an increasing trend in global demand and predicted to achieve 15.25 billion $ turnover by 2026. Economic importance of HA lauds primarily due to its sustainable water retention capability by retaining moisture in the skin surface. The characteristics of HA are biodegradable and its biocompatibility appeals for various applications in biomedical and cosmetic industries. HA was discovered by Karl Meyer and John Palmer in 1934 [8] by isolating it from the vitreous body of the cows. It is also ubiquitously present in the extracellular matrices

of all mammalian tissues offering structural support and rigidity. In the human body, HA is found in several soft connective tissues, vitreous humor and synovial fluid. HA hydrogels are being synthesized into scaffolds that helps in tissue regeneration [9], aiding to the wound healing due to its non-immunogenic properties. As HA is highly hydrophilic it is desirable to use in a wide range of skin problems including wrinkles, anti-aging, skin hydration etc. and it is being used as an active ingredient in a large number of cosmetic formulations [10]. Lower Molecular Weight HA (LMWHA) is employed in the production of inflammatory mediators [11]. Also LMWHA is applicable as a capsular material for drug carrier extending their pharmacological half-life activity at par with Poly-Ethylene Glycol encapsulated (PEGylated) drugs [12]. But the application of higher molecular weight HA (HMWHA) deserves high degree of attention in biomedical industry. The affinity for CD44 (Cluster of Differentiation 44) receptor is very high for HMWHA and plays additionally mediating role in angiogenesis for wound healing. HMWHA as a potential biomaterial, also possess better durability for most of the cost-effective applications like development of scaffolds, tissue engineering allied materials, etc. Traditionally HA was extracted from rooster combs owing to higher concentrations compared to other natural sources. One major drawback in the extraction process was degradation of hyaluronan caused by endogenous hyaluronidase activity in animal tissue [13]. Moreover, extraction of HA from animal sources and its application in biomedical and pharmaceutical field is being opposed by various countries and organizations citing health hazard due to viral contamination [13]. Hence, microbial fermentation of HA synthesis had gained attention over last 3 decades.

Naturally *Streptococci sp.* was evolved with the synthesis of polymeric HA in million Daltons range in parallel with the structurally complicated biomass synthesis [14]. *S. zooepidemicus* was previously reported to be thermodynamically feasible with the production of other catabolites

such as Lactic acid (LA) and mixed acids in addition to the anabolic burden [14]. Microbial HA production is the topic of interest on metabolic perspective, since the carbon flux competes for the synthesis of multiple products.

Initially, microbial fermentation of HA was achieved using *Streptococcal* bacterial system. Later various wild type strains of *Streptococcus sp.* harboring type-1 *has synthase* gene such as *S. zooepidemicus, S. thermophilus* [15], *S. pyrogenes, S. equisimilis, S. uberis* [16] and from other genera comprising type-2 *has synthase* such as *Pasteurella multocida* [17] were employed to produce HA. Molecular weight of HA is a key attribute in deciding the commercial potential of the developed product. Molecular cloning of *has* family genes in an alternate host, determined to be stable and advantageous for downstream processing were attempted in *Bacillus subtilis* [18], *Escherichia coli* [19], *Pichia pastoris* [20], *Lactococcus lactis* [21], *Corynebacterium glutamicum* [22], and *Agrobacterium sp.* [23]. Those methodologies were proven to successful in HA synthesis but uncertain about the mechanism of HA polymerization and the role of UDP precursors. Very few process control based approaches had addressed the role of physiological and operating parameters influencing the molecular weight of HA.

Appropriate regulation of specific growth rate of microorganism was reported to influence HA molecular weight and titer by various research groups previously. Several process engineering approaches carried out by different research groups adopted a methodology in varying μ to record the outcome in HA MW. Improvement of culture conditions, media supplements attempted was one of the first report entails on the effect of μ on HA molecular weight and observed that HA MW was highest (2.40 MDa) at the lowest recorded μ_{max} of 0.45 ± 0.15 h^{-1} for *S. zooepidemicus*. A similar observation i.e. inverse relationship between μ and MW was later confirmed in *S. zooepidemicus* [25]. Other recombinant hosts harboring *has* operon such as

116 *L. lactis* also exhibits similar correlation, where the continuous cultivation was carried out at
117 0.066 h^{-1} dilution rate resulted in a improved molecular weight of 2.6 MDa [26]. Also proposed
118 increment in the intracellular molar ratio of Uridine-di Phosphate D-glucuronic acid (UDP-
119 GlcUA) and Uridine-di Phosphate N-acetyl-D-glucosamine (UDP-GlcNAc) obtained at a lower
120 μ range was another prime factor leading to augment HA MW in *L. lactis* host. All the
121 investigations pertaining to the specific growth rate points at the stringent control over μ at an
122 extended period of time, which would guarantee the HA MW preferably higher. Operating at
123 lowermost μ values, the organism gets constrained in allocating carbon flux to the synthesis of
124 HA over other end products, especially for Lactic acid. In general, fed-batch approaches are ideal
125 strategy in the sustained production of biopolymers, antibiotics, etc under restricted/stressed
126 environment.
127 Operational control of fed-batch process is generally simpler if predetermined feed is
128 supplemented by predicting the futuristic substrate requirement of an organism [27].
129 Feedforward (FF) strategy is well appreciable in the cases where a balanced growth leading to a
130 continuous increment in substrate and product concentrations upon prolonged feeding [28]. But
131 in the cases like competitive HA biosynthesis with other end products demands the corrective
132 control output in the form of regulated feed rate dictated by the controller element. Real-time
133 process input by a soft sensor is another foremost important factor to illustrate the process
134 variable and address the adequacy to the Supervisory Control and Data Acquisition (SCADA)
135 for the controller action.
136 Process Analytical Technology (PAT) guided approach emphasizes the deployment of soft
137 sensors to monitor the intended bioprocess for a consistent product output [29]. Signal acquired
138 from the soft sensors deciphers the crucial process inputs, highlighting the control of process

parameters to be regulated in a desirable range. Monitoring of *S. zooepidemicus* growth by soft sensors developed based on fermentation calorimeter, capacitance probe and exhaust gas analyzer measurements was successfully accomplished by our research group [14,30]. Metabolic heat production is an inherent property of all living organisms and its real-time measurement (calorimetry) could be useful in tracking metabolic activity of on-going bioprocess systems [30]. Application of calorimetry as a PAT tool was successfully established for real-time monitoring of metabolic activity in different microbial systems [31,32,33] and in gaining deep insight on thermodynamics of microbial growth [14]. However, design and development of soft sensors based on real-time calorimetric measurements and its application for process control is scarcely reported in literature, especially for biopolymer synthesis like HA. Strategy based on μ control would be simpler and ideal for improving HA MW, can be discerned from previous findings. In this present study, a soft sensor for specific growth rate was modeled using the real-time metabolic heat rate measurements for monitoring and control of HA production. This investigation focuses on the advantages and suitability of the developed soft sensor (specific growth rate estimator, μ_{est}) towards monitoring of HA production and its subsequent substrate feed rate control. The robustness of developed feedback (FB) control strategy is compared with the conventional FF control, its outcome in the final titer, MW and Polydispersity index (PDI) of HA.

Results

Calorimetric monitoring of *S. zooepidemicus* growth

Cell physiological activity and kinetic parameter estimation deciphered from metabolic heat rate measurement was already reported for bacterial and yeast microbial systems [31,32,33]. Fermentation calorimeter employed in this study is advantageous in terms of its high sensitive

heat rate measurement and its response time is in 10 – 15 seconds compared to other heat-flux calorimeters. In this present investigation real-time signals viz. heat rate and CER confers reliable elucidation of different phases of *S. zooepidemicus* growth. Also heat yield coefficient of CO_2 was found to be increasing from 443 kJ/mol at the start of exponential phase to 1125 kJ/mol. at later stages confirming fermentative type metabolism. Respirometric data offers prominent process information about the significant amount of anaerobic CO_2 produced disproportionate to the heat generated in the system, which classify the HA production process is a facultatively anaerobic in nature [34,35,36]. Unanimously in all the reactor runs, the batch and fed-batch (Figure 2A – 2C, Figure 3A – 3C) growth profiles of *S. zooepidemicus* were found to be distinct, suggesting that the specific growth rate ($\mu_{offline}$) was influenced by exponential feeding. The estimated range of specific growth rate values ($\mu_{offline}$) during batch and fed-batch phase (Table 3 & 4) were found to be 0.32 – 0.41 h^{-1} and 0.056 – 0.11 h^{-1} respectively. $\mu_{offline}$ values during growth phase is significantly (4 times) higher than the fed-batch phase substantiating the effect of substrate-limited growth achieved by exponential feeding. The final titers and specific productivities of biomass, LA, HA during FF (Table 3) and FB (Table 4) control strategy showed significant variation at different μ_{SP} runs. The observed values were found to be highly concordant in both FF and FB approaches.

Development of heat rate based μ estimator

The developed μ_{est} was modeled based on the biological heat dissipation from metabolic reactions coupled with biomass synthesis. The biological heat rate (q_B) values recorded over a frameshift with respect to the cumulative heat dissipated (Q_t) in the system serves to be the critical factor in determining μ_{est}. Estimated Batch-phase $Y_{Q/X}$ was substituted in the Eqn. 4, which would be suffice to deduce the real-time μ_{est} in the production phase. Based on the Eqn. 9

and 11, substrate feed rates during FF and FB controls were tightly regulated at different μ_{sp}. A comparative assessment of the developed μ_{est} with the corresponding dynamic $\mu_{offline}$ values were dealt and a good synchronization (Figure 4A – 4C & Figure 5A – 5C) was observed for the span of 7 h approximately. FF control strategy was observed to be ineffective in regulating the specific growth rate to the desired μ_{sp} (> 0.1 h^{-1}), which could be witnessed from the significant variation in $\mu_{offline}$values. Similarly, FB control at $\mu_{SP} = 0.15\ h^{-1}$ was not effective and $\mu_{offline}$ values were found to be significantly lower than desired setpoint value i.e. $0.15\ h^{-1}$.

Feedforward (FF) and Feedback (FB) control strategies

Feeding of glucose was started between 8 – 9 h during every fed-batch operation in both strategies (FF and FB) and continued till its completion. The residual glucose concentration in all the FF and FB control experiments were found to be too low for detection, emphasizing that the glucose was actively metabolized as indicated by heat rate signal (Figure 6A – 6C & 7A – 7C). FF control strategy adopts conventional methodology, which involves the consistent feeding of glucose at predetermined rate (Eqn. 8) and the pulsed feeding continues without discerning its outcome. The predetermined feed rates (F_0) were estimated to be 8 mL/h ($\mu_{SP} = 0.05\ h^{-1}$), 12 mL/h ($\mu_{SP} = 0.1\ h^{-1}$), 18 mL/h ($\mu_{SP} = 0.15\ h^{-1}$) appropriately for the respective μ_{SP} runs (Figure (6A – 6C)). The principle of the developed FB control strategy (Eqn. 12) was based on the biological heat rate inputs i.e. process inputs recorded in the SCADA (Fig. S2). The noisy perturbations (Fig. 7) observed in the feed rates during FB strategy could be solely attributed to the performance of PID controller. The working principle of the PID controller was briefly discussed in the 'Feedback control strategy' section. PID tuning parameters determine the sustained perturbations in the glucose feed during fed-batch phase. In the present study the controller gain, k_C was maintained at 2 for all the experiments, especially designed to operate

closer to its μ_{SP}. Controlled feeding of glucose by FF and FB strategy at appropriate μ_{SP} values resulted in the significant improvement of the final titers of HA and other end products. It is evident from the FF and FB control runs, that LA production was relatively lesser (Tables 3 & 4) at lower μ_{SP} (Figures 8A & 8B). Difference in LA concentrations were significantly low in both (FF and FB) approach and could be indirectly related to the operated μ_{SP}. The lowest μ_{SP} i.e. $0.05\ h^{-1}$ shows resulted on good reduction in the LA formation, indicating that the major carbon flux might be channeled towards HA synthesis. Increase in HA concentration from 3.15 to 4.22 g/L for the μ_{SP} corresponding to 0.15 to $0.05\ h^{-1}$ observed in FB strategy would substantiate this claim. However, contrary results were observed in case of FF strategy especially the reduction in HA concentration from 4.73 to 3.57 g/L for increase in setpoints μ_{SP} ranging values from 0.15 to $0.05\ h^{-1}$. Interestingly, the final biomass concentration was observed to increase in both FF and FB control runs for an increase in μ_{SP} from 0.05 - 0.15 h^{-1} (Table 3 & 4)

Molecular weight (MW) and Polydispersity Index (PDI)

A noticeable improvement in the MW of HA was observed for decrement in μ_{SP} from 0.15 h^{-1} to 0.05 h^{-1} in both the strategies (FF and FB). The computed MWs were averaged to the final 3 samples for obtaining the overall mean MW of the deployed strategy. In FB strategy mean MWs estimated was found to be 2.98, 2.73 and 2.48 MDa corresponding to the μ_{SP} of 0.05, 0.1 & 0.15 h^{-1} respectively (Fig.9B). A similar trend in increment of MWs 2.95, 2.54 and 2.42 MDa was observed in case of FF strategy for 0.05, 0.1 and 0.15 h^{-1} μ_{SP} runs respectively (Fig. 9A). PDI was estimated from the chromatogram of HA samples by adopting the methodology as previously reported [37] and was found to be in the range 1.55 to 1.73 (FB) and 1.77 to 1.83 (FF). PDI values of HA samples obtained from FB control runs were reportedly of superior indices compared to the FF strategy.

Discussion

Specific growth rate estimator

The modeled specific growth rate of organisms tabulated (Table 1) employing various process analyzers can be deployed according to the suitability of the investigating system. It depends upon the ability of the soft sensors to decipher the real-time process variables are key to its applicability. For example, dielectric spectroscopy based μ interpretation of bacterial cultures are unsuitable owing to lower sensitivity for organisms less than 10 micron dimension. In a similar line CER/OUR based control process inputs may be unpredictable during production phases of an organism, although they are highly reliable during growth phases. But calorimetry based investigation functions based on the thermodynamics of cellular metabolism and gibbs free energy dissipation is imminent for any living system. Heat rate signal is a reliable indicator of much simpler metabolic activities and responds to the calorimetric determination. Fermentation calorimeter employed in this study therefore determines the heat rate as low as 6.73 mW/L and good enough to predict the specific growth rates as well. Compared offline values ($\mu_{offline}$) with the μ_{est} signal at various PID tunings were presented in table 2. The tracking of μ_{est} at different phases was found to be a significant development in HA production process in spite of its extreme rheological/viscous nature.

PID control characteristics

The control of specific growth rates during fed-batch (production) phase ($\mu_{SP} < \mu_{max}$) was achieved by the feed rate dictated by FF and FB strategies. The FF strategy provides straight-forward output and holds uncertain about the dynamics of process input exhibiting the overall μ_{est} to be 0.062 h^{-1}, which was slightly greater than $\mu_{SP} = 0.05\ h^{-1}$. In case of other control runs (μ_{SP} = 0.1 & 0.15 h^{-1}), FF strategy without process input was a challenging bid and

resulted with lowered specific growth rate values, 0.066 h^{-1} and 0.11 h^{-1} respectively. Predetermined feed rate works well in the cases where substrate affinity (K_S) constant between the organism and substrate are determined to be lower i.e. superior assimilation of excess substrate supplied in the reaction broth [37]. Moreover, high possibility exists for increased influx of glucose during the exponential feeding strategy [38] that could inhibit the organism growth. Continuous drop in μ_{est} can profile ($\mu_{SP} = 0.15\ h^{-1}$) can be noticed, which could be attributed to excess feeding. It is also evident from sequential slump in $\mu_{offline}$ values depicted in Figure 4A – 4C. However, deployment of FF control strategy was managed to achieved an improved production of HA and end products (Fig. 8A).

Relatively better control in $\mu_{offline}$ was achieved in FB strategy in contrast to FF approach. Incorporation of PID control resulted in a convincing output in the regulation of μ_{est}, actuated by the variable speed pump except a slight deviation observed for control run at $\mu_{SP} = 0.15\ h^{-1}$. But, the control of specific growth rate was observed to be robust at lower setpoints i.e. $\mu_{SP} = 0.05$ & $0.1\ h^{-1}$. The controller gain, k_c defined to be the ratio of glucose feed rate and μ_{est} developed was set to 2 throughout the reactor run. Dead time, τ_I was set to 10s, 100s and 200s (Integral value can be computed from the inverse of dead time) maintained along with the proportional term. Keeping k_c constant, other PID elements (especially τ_I) were manipulated for every 2 – 3 h during fed-batch operation and analyzed for its influence on the feeding profile. The changes adopted in the PID control elements were determined to reflect in the manipulation of feeding profiles. Integral time of 100s was best suited controller tuning and found to be robust for the deployed system. This observation can be confirmed from the tracking errors at different setpoints were relatively lower than other tuning parameters as illustrated in table 2. The comparison plot of μ_{est} & $\mu_{offline}$ depicting the dynamic changes (Figure 4A – 4C (FF strategy)

277 and Figure 5A – 5C (FB strategy)) was tracked well by the modeled real time μ_{est} with a good
278 precision. However, the PID controller suffers limitation at higher setpoints say 0.15 h^{-1} due to
279 the internal metabolic constraints of an organism. The ability of organism to grow at higher μ
280 would suffer challenging due to the extrusion of million Dalton size HA over the cell surface and
281 continuous synthesis of LA additionally. Inherently the growth rate of an organism gets reduced
282 during the production phase. The PID controller is of purely mechanistic in nature, unable to
283 decipher the metabolic shift from growth to production phase and dependent upon the real-time
284 estimates. Metabolic limitations due to innate capability of organism to grow at the desired high
285 specific growth rate conditions, the usage of any type of controller can be disregarded. The
286 applicability of the PID controller well suited for condition, $\mu_{SP} < 0.15\ h^{-1}$,which actuates the
287 feed rate robustly. Also, it becomes difficult to feed the organism at lower most μ_{SP} values due
288 to its thermodynamic constraint.

289 **Evaluation of feed rates and its influence over the synthesis of various end products**

290 Based on the overall assessment of the dynamic end product profiles of all control (FF and FB)
291 runs, it could be witnessed that the regulated feed rate significantly impact the overall metabolic
292 machinery of the organism. Both FF and FB control runs (at different μ_{SP} conditions) exhibited
293 good synchronization between calorimetry and respirogram signals. The batch phase growth of
294 *S. zooepidemicus* utilizing 30 g/L of glucose in all the reactor runs was found to be conserved
295 and the rate of assimilation of glucose during log phase could be highly reproducible. In many
296 literatures, it was well reported that the exhaustion of limited substrate is remarked with a sharp
297 sudden slump in heat rate signal, accompanied with a DO spike [31]. In this investigation,
298 glucose feed was initiated well before its exhaustion leading to the smooth continuation of
299 metabolic assimilation, as evident from the continuity in the calorimetric signal (Fig. 2A – 2C &

Fig. 3A – 3C). Calorimetric signal possesses better reliability in tracking metabolic activity than CER output [30], due to the decreased cell viability in the later stages of culture growth. A steeper slump in the respirometric profiles after active growth phase may not be reliable for further control application. Very few investigations reported the impact of LA synthesis on HA productivity and hinted that LA production is highly likely to be produced by the organism compared to complex HA biosynthesis. An inverse relationship was already reported between the yields of HA and LA [26]. Our research group previously reported a maximum of 70 % of total carbon input gets diverted towards LA formation [30]. In the present investigation, LA titer at the end of the batch phase was more than 50 % of the total carbon input. All these observations prove that the glycolytic pathway is highly predominant for carbon assimilation and shows easiness in producing LA by fermentation. Moreover the orchestration of *has* operon activity is also dependent upon the fermentative production of LA, conserving the energy intermediates essential for HA synthesis.

In FF strategy, the increment in the biomass concentration was concomitant with the increase in the titers of other end products. Biomass and other end product concentrations were observed to increase gradually at an increase in feed rates corresponding to different μ_{SP}. At 0.15 h^{-1}, the optimal biomass (4.60 g/L), HA (4.73 g/L), LA (31.51 g/L) concentrations were achieved and higher proportion of carbon flux was predominantly diverted towards LA formation (LA titer several fold higher than other end products and HA). Notably, the rate of biomass generation and HA formation was unlikely to be inhibited by the increase in LA efflux. Yield of HA per g. of biomass was found to be closer to 1 in all μ_{SP} runs (Figure 8A). This is substantiated by the highest HA titer 4.73 g/L was achieved in spite of acute LA synthesis during fed-batch phase.

Final titer of biomass and end products achieved in FB strategy were significantly lower than that of the corresponding FF combination. This proves the tightly regulated feed limits the synthesis of end products and also reinstates house-keeping activities more effectively. For instance the range of feed regulation between 8 – 11 mL/h was carried out during $\mu_{SP} = 0.05\ h^{-1}$, but the differences in biomass synthesis and LA formation between FF and FB strategy was found to be significant (Table 3 & 4). The optimal HA concentration of 4.22 g/L was achieved in FB strategy, comparatively lower than FF strategy. But the specific HA productivity q_{HA} during fed-batch phase was found to be significantly higher than the corresponding q_{HA} of FF strategy (Table 3), proving that the organism favoured HA synthesis more likely in the FB strategy. Tighter regulation at lower μ_{SP} can limit the glycan precursor ratio optimal for higher molecular weight as elucidated previously [26]. LA concentration reached maximum of 26.74 g/L at $\mu_{SP} = 0.15\ \mathrm{h}^{-1}$ and also less favourable as compared to the FF strategy. In overall conclusion, HA titer gets influenced with the substrate flux continuously fed into the system. Other end product formation and its rate does influencing HA MW was discussed subsequently.

Effect of specific growth rate (μ_{est}) on HA molecular weight

Improvement in the MW of HA is actuated by the continuous activity of *has* operon. The sustained synthesis of HA is dependent upon the intracellular UDP precursor pools and the availability of Uridine di phosphate Glucuronic acid (UDP-GlcUA), which is the rate limiting step reported in many articles. Anabolic nature of HA synthesis consumes more energy than other byproducts. The rate of HA polymerization was reportedly found to be 60 monosaccharide units added per minute and grows into 2 MDa macromolecule in 3 h duration [26]. Therefore it is

more important that the HA polymerization should be ensured to continue without prematurely termination.

The HA MWs reported in Figure 9A – 9B clearly substantiates that the lower μ_{SP} control would support the extended polymerization in HA MW. The highest MW of 2.98 MDa and 2.94 MDa were obtained at a lowest projected μ_{SP} value of 0.05 h^{-1}. Both the strategies yielded the MW in a similar range exhibiting good reproducibility in the control strategy. Also control of μ_{SP} say 0.05 h^{-1} in both the strategies (FF & FB) was accompanied with least turnover of other products (DCW & LA). At higher μ_{SP}, although the final product turnover was high, but HA MW seems to be reduced. Lower PDI values obtained for FB strategy proves that the MW fraction obtained were more uniformly distributed than the other strategy. At a reduced growth rate, the available GlcNAc precursor from glucose gets diverted towards functional *has* machinery. The LA production also support *has* operon activity by supplying redox cofactors to oxidize the glucose intermediate into GluUA catalyzed by *hasB* [39]. Comparatively low HA titer obtained in the FB reactor runs than the FF strategy was another indication that the relative MWs in FB strategy would be higher than the FF strategy. This establishes the inverse correlation between HA concentration and corresponding MWs. The outcome of higher MW in a regulated feed proves that the glucose flux prioritize in the synthesis of UDP precursors essential for biomass and HA production by skipping the glycolytic pathway. This can be inferred from the reduced LA titers in comparison with the FF strategy. Moreover the control of μ_{est} at lower range during viscous production phase appears to be challenging effort. Also at lowered specific growth rate, the UDP precursor pool in the cytosol would be predominantly richer in UDP-GlcUA than UDP-GlcNAc [30]. It was well reported that turnover of UDP-GlcNAc precursor is the rate limiting step in the functioning of *has* operon guiding the extrusion of higher MW HA in the capsular surface.

Conclusion

This present study proves that the sustained control of specific growth rate of *S. zooepidemicus* for more than 7 – 8 h employing an indirect inferential control of metabolic heat rate as a process signal and also remains as the first of its kind. Calorimetric signal was observed to be robust in tracking various phases in growth and fed-batch phases of HA production by *S. zooepidemicus*. Robust control of specific growth rate at low setpoints yielded improved HA MW especially at $\mu_{SP} = 0.05\ \mathrm{h}^{-1}$. A simple PID based FB strategy was found to be efficient in the robust control of process parameters, instead proceeding with a predetermined FF control strategy. This presented study encourages the application of calorimetry as a PAT tool at industrial scale, since increased metabolic heat production could be observed at large scale bioreactors (high surface to volume ratio) ensuring reliable monitoring and control. Moreover, the elucidation of other key process variables/kinetic constants by deconvolution of calorimetric signal widens the scope of the developed feed control strategy.

Materials & Methods

Microbial strain and media

Streptococcus equi. subsp. zooepidemicus 3523 (Gram Positive) was procured from Microbial type culture collection (MTCC), Institute of Microbial Technology (https://mtccindia.res.in/files/masterculture/mtcc_catalog.pdf), Chandigarh (India) and preserved in Todd-Hewitt (TH) agar slants. A single mucoid colony was pre-cultured in TH broth supplemented with 5 g/L brain heart infusion and incubated overnight at 37 °C and 180 RPM.

Calorimeter setup and principle

Heat compensation fermentation calorimeter (Biojenik Engineering, Chennai, India) developed in-house was employed in this study to measure the biological heat rate, q_B. The reactor vessel is of double jacketed type: the outer jacket holds vacuum sealed in it to avoid heat loss through the lateral surface. The temperature sensors (Isothermal Technology Ltd, Merseyside, England) acquiring the process inputs at reaction broth and jacket inlet (T_r and $T_{j,in}$) are of highly sensitive (1 mK range) serves as process variable to their respective controls. The inner jacket circulates silicon oil at a regulated temperature setpoint and acts as a thermal insulation additionally. The heat rate measurement principle was reported in detail in our earlier study [30], which actuates 2 independent PID controls in tandem maintaining T_r and $T_{j,in}$ at their respective setpoints. The 1st PID control adjusts the wattage output of Compensation Heater (CH) (Biojenik Engineering, Chennai, India), thus controlling T_r more precisely. Reaction enthalpy due to chemical/biochemical activity can be precisely measured from the reduction in power output of CH. The 2nd PID loop in the cryostat (Julabo GmbH, Seelbach, Germany) manipulates the temperature of silicone oil flowing through inner jacket. An additional PID cascade loop developed in the LabVIEW platform provides variable setpoints to the PID loop (2nd PID controller) of the cryostat, thus reducing the effect of ambient temperature fluctuations. Data acquisition of other process inputs such as pH, DO, stirring rate, torque were integrated in the LabVIEW based DAQ module (NI cRIO 9075, National Instruments, United States). The reactor and its interface are also equipped with separate pH, temperature and DO controls. Non-biological heat rates due to different operating parameters as shown in Fig. S1 were quantified/calibrated and included in the dynamic energy balance to avoid disturbances to the

calorimetric signal [30]. The dynamic energy balance adopted in our previous research work in the calorimeter was represented in the following Eqn. 1

$$m_w C_p \frac{dT_r}{dt} = q_C - q_J - q_E + q_S - q_A + q_B$$

---Eqn. 1

The operating parameters were maintained at an optimum level throughout the reaction and the cumulative contributions of all non-biological heat rates were maintained to be zero prior to the microbial inoculation. The biological heat rate, q_B can be deduced from the output of CH and baseline heat rate as shown in eqn. 2, noise filtered by moving average of every 100 data points and recorded for every 5 s intervals.

$$q_B = q_{Baseline} - q_C$$

--- Eqn. 2

An improved resolution of 6.73 mW/L was achieved by incorporating various reactor housing steps. In addition to this enthalpy balance incorporating different chemical species engaged in the process was already reported in detail [14]. The data can be helpful for the scaling-up in future.

Carbon dioxide Evolution Rate (CER) determination

Exhaust Gas Analyzer (Ultramat 23, Siemens AG, Berlin & Münich, Germany) utilizes infra red (IR) absorption detector for measuring the gaseous phase CO_2 concentration ($y_{CO2,out}$) and the values were recorded at every 5 s intervals. Real-time CER computation from $y_{CO2,out}$ can be estimated from the following relationship (Eqn. 3)

$$CER, {}^{m.mol}/_{L.h} = \frac{\dot{m}_a}{V_R}\left[y_{CO2,out}\left(\frac{y_{inert,in}}{y_{inert,out}}\right) - y_{CO2,in}\right]$$

---Eqn. 3

Where, $\dot{m}_a$ = Mass flow rate of air, LPM and V_R = Reaction working volume, L, $y_{inert,in,out}$= Gaseous phase nitrogen concentration.

Media constituents and Process conditions

All the reactor runs were performed in the fermentation calorimeter at a working volume of 3 L with a preculture comprising 8% (v/v) of the reaction broth. Overnight grown (≈ 18 h) shake flask culture was aseptically transferred into the calorimeter/reactor containing production media. The composition of the media is as follows (in g/L): Yeast extract 10, $MgSO_4.7H_2O$ 3, K_2HPO_4 1.5, KH_2PO_4 3, NH_4Cl 5. Initial glucose concentration of 30 g/L was supplied for all the reactor runs. Batch phase was carried out for 10 – 12 h before proceeding for the control of specific growth rate through controlled feeding of the limiting substrate (glucose).

Development of heat rate based specific growth rate estimator (μ_{est})

Gibbs free energy dissipation is a ubiquitous phenomenon, representing even a simplest life form in the planet. Heat rate evolved from the reaction broth is resultant enthalpy [14] from overall cellular metabolism (catabolic and anabolic), and the growth kinetic parameters could be deduced from heat yield coefficient as given in the eqn. 4

$$Y_{Q/X} = {q_B}/{r_X} = {q_B}/{\mu.X}$$

---Eqn. 4

Resolving eqn. 4 by integrating between the limits x: $X_0 \rightarrow X_t$ and t: $0 \rightarrow t$,

$$X = X_0 + \frac{Q_t}{Y_{Q/X}}$$

---Eqn. 5

Where q_B, biological heat rate (W/L), X_o, biomass concentration at the end of batch phase (g/L), $Y_{Q/X}$, biomass heat yield coefficient (kJ/g) and Q_t, cumulative heat at that time instant (kJ/L).

Rearranging Eqn. 4 into Eqn. 5, the relationship between $Y_{Q/X}$ and μ could be obtained (Eqn. 6). Considering the constant volume during fed-batch reactor operation, Eqn. 5 gets modified into Eqn. 6.

$$Y_{Q/X} = \left[\frac{q_B}{\mu\left(X_0 + {Q_t}/{Y_{Q/X}}\right)}\right]$$

---Eqn. 6

The specific growth rate estimator (μ_{est}) model was developed, (Eqn. 7) considering constant reactor working volume (V_R) till the completion of fed-batch reactor operation. This assumption holds practically true as the overall cumulative feeding volume did not exceed beyond 5 % of V_R.

$$\mu_{est} = \frac{q_B}{Y_{Q/X}.X_0 + Q_t}$$

---Eqn. 7

During engagement of glucose feed, q_B and Q_t values were recorded at a frameshift of 30 min. interval. The noise pretreated signal (mean averaged at every 100 data points) was utilized to compute the estimation of real-time μ_{est}. Dry cell weight (DCW) estimation would be helpful in the calculation of offline specific growth rate ($\mu_{offline}$) values, which serves as a bench mark for substantiating the reliability of model estimate (μ_{est}) developed in this study. μ_{est} values were connected to the PID loop, eliciting subsequent control over the regulated feed of glucose were discussed elaborately in the 'Feed rate' section. Track error computed between μ_{sp} and μ_{est} would testify the sensitivity of the controller developed (Table 2). Heat rate based μ_{est} model was already reported for *E. coli* [31], *S. cerevisae* [32] and *K. marxianus* [33].

Feed rate control

Feedforward strategy

Feed forward strategy admits the supply of excess feed disproportionate to the nutritional requirements of microbial growth [27]. It predetermines the feed of limiting substrate based on the kinetic parameters of the batch growth phase. The initial feed rate can be computed by Eqn. 8

$$F_0 = \frac{X_0 V_0 \mu_{sp}}{S_0 Y_{X/S}}$$

---Eqn. 8

Where X_O, biomass concentration at the end of batch phase (g/L) ;V_O, reactor volume at the end of batch phase (L) ;S_O, is glucose concentration in feed stream (g/L) and $Y_{X/S}$, biomass yield (g/g). Glucose feed was carried out using a high precision pump (Watson Marlow 120U, Falmouth, Cornwall, U.K) during fed-batch phase operation. Exponential rate of feeding can be achieved by the following expression (Eqn. 9)

$$F_{FF} = F_0 e^{\mu t}$$

---Eqn. 9

Feedback strategy

FB strategy monitors the microbial growth by the incorporation of reliable process inputs and permits regulated substrate feed into the reactor. Therefore, functioning of the manipulating variable i.e. variable speed precision pump is dictated by the process control elements, thus maneuvering the organism growth. The advantage of this method is that the inherent dynamics of cell growth during fed-batch phase gets adjusted to the proposed setpoint due to the tighter regulation of the glucose feed [40,41]. Error (difference between the setpoint and process variable) gets computed by the controller based on Eqn. 10

$$\varepsilon(t) = \mu_{sp}(t) - \mu_{est}(t)$$

---Eqn. 10

While implementing this strategy, a slighter modification has been done to the controller algorithm. Proportional, integral and derivative terms were directly included to the exponent term of feed rate equation as shown in Eqn. 9. Exponential feed rate in this phase was regulated by PID output ($PID(O/P)$) and as represented by Eqn. 11

$$PID\,(O/P) = k_p\varepsilon(t) + \frac{1}{\tau_i}.\int_0^t \varepsilon(t).dt + \tau_D.\frac{d}{dt}.\varepsilon(t)$$

---Eqn. 11

Based on the controller output, feed regulation was carried out using a high precision pump (Watson Marlow 120U, Falmouth, Cornwall, U.K). Exponential glucose feeding based upon controller response is aliased with FF and FB components together as represented in Eqn. 12

$$F_{FB} = F_0 e^{(PID\,(O/P)).t}$$

---Eqn. 12

Schematic representation of μ_{est} model and its input into the PID loop, subsequent feeding into the reactor regulated by variable precision glucose pump was shown in Fig. 1.

Analytical estimation

Reaction broth samples were collected at regular time intervals and stored at 4°C. Cell bound HA from the reaction broth samples were treated with 0.1% (v/v) sodium dodecyl sulphate (SDS) to strip-off HA from the cell membrane. The soluble fraction containing HA was separated by centrifugation at 6160×g for 10 min. Retained supernatant was utilized for the estimation of HA, LA and residual glucose concentrations. Biomass concentration was determined from the pellet

by OD_{600} measurements and interpreted with the standard plot developed for OD vs DCW correlation (1 Absorbance unit (OD_{600}) = 0.33 g/L biomass) obtained for *S. zooepidemicus*. HA solubilized in the supernatant was precipitated by the addition of 4 volumes of absolute alcohol. HA precipitate was washed thrice with ethanol to enhance its purity. The HA pellet was stored in saline (0.9 % w/v NaCl) overnight for solubilization. The CTAB assay [42] was carried out to estimate dynamic HA concentration in the samples over various time intervals. The assay procedure involves the incubation of solubilized HA samples with equal volume of 0.1 M Phosphate buffer at 7 pH and 37ºC for 15 min. Followed by which twice the volume of CTM solution (2.5 g of CTAB dissolved in 100 mL of 2% (w/v) of NaOH) was added and incubated at 37ºC for 10 min. Absorption spectra was read at 600 nm and compared with HA standard plot calibrated at its working range to deduce HA concentration in experimental samples. Analyte (Glucose and LA) concentrations were estimated by HPLC methodology [37] (Prominence Modular HPLC, Shimadzu Systems, Kyoto, Japan) employing analytical column specific for the estimation of monosaccharides/organic acids (Rezex RHM- monosaccharide H+ column, Phenomenex Inc, California, USA). Degassed Mobile phase containing 5 mM H_2SO_4 was set to flow through the column in an isocratic mode at 0.5 mL/min. Refractive Index Detector (RID) reads absorption peaks at 14.16 min. and 19.7 min. corresponding to the pure glucose and LA respectively. Area under curve determined for the working standards were interpolated for the samples withdrawn at various time intervals to obtain respective analyte concentrations. Alcohol/acetate and other compounds were undetected.

Molecular Weight and PDI estimation of HA

Size exclusion chromatographic column (Polysep 6000, GFC Column, Phenomenex Inc, California, USA) sieves and segregate polymers based on their molecular weight. Dextran

polymer standards ranging between 100 kDa – 8 MDa was utilized for the development of calibration model. Mobile phase containing de-gassed 0.2 M $NaNO_3$ was set to flow through the column at 0.5 mL/h in an isocratic mode. The retention time recorded for the biological samples illustrate the molecular weight of the synthesized HA from the developed calibration model. Polydispersity Index (PDI) is a ratio between the molecular weights of number averaged and weight averaged, also represents the degree of homogeneity in the molecular weight of a polymer. Computation of PDI was carried out separately from the generated chromatogram as reported previously [37]. PDI index '1' represents monodispersive nature of the polymer length and also considered to be ideal for any polymer.

Table 1 Elucidation of μ estimator, signals, process variables interpreted from different process analyzers

Process Analyzer	Signals	Process parameter	μ estimator/modeller
Biocalorimetry [43]	Heat rate signal	Metabolic heat rate/Enthalpy	$\mu_{est} = \frac{q_m}{X_0 V_0 Y_{Q/X} + (Q_t - Q_0)}$
Dielectric spectroscopy [40, 41]	Capacitance signal	Viable cell concentration	$\mu_{est} = \frac{\ln(\Delta C_{t,n}) - \ln(\Delta C_{t,n-1})}{(t_n - t_{n-1})}$
Respirometry [44]	OUR/CER	Respiratory quotient,	$\mu_{est} = \frac{r_X . Y_{CO_2/X}}{X . Y_{CO_2/X}}$

Table 2 Tracking errors, PID parameters and its influence over μ_{est} over different μ_{sp}

PID Parameters			$\mu_{sp}(h^{-1})$	$\mu_{est}(h^{-1})$	$\mu_{Offline}(h^{-1})$	Average tracking error (%)
Controller gain, k_C	**Integral time, τ_I (s)**	**Derivative time, τ_D (s)**				
2	10	0	0.05	0.039	0.06	22
	100	0		0.051	0.057	02
	200	1		0.048	0.047	04
2	10	0	0.1	0.061	0.106	39
	100	0		0.115	0.087	15
	200	1		0.084	0.088	16
2	10	0	0.15	0.089	0.103	41
	100	0		0.099	0.092	34
	200	1		0.078	0.094	48

559 Average tracking error was computed using the relationship $\frac{(\mu_{sp}-\mu_{est})\times 100}{\mu_{sp}}$

Table 3 Final titers, yield coefficients, growth and formation rates of biomass, HA and LA were tabulated during distinct batch and fed-batch phases of the FF control runs carried out at different μ_{SP}

μ_{SP}(h^{-1})	Biomass conc. (g/L)	$Y_{X/S} \times 10^{-2}$ $\left[\frac{g.Biomass}{g.Glucose}\right]$	$\mu_{offline}$, (h^{-1})		HA conc. (g/L)	$Y_{HA/S} \times 10^{-2}$ $\left[\frac{g.HA}{g.Glucose}\right]$	q_{HA} $\left[\frac{g}{g.h}\right]$		LA conc. (g/L)	$Y_{LA/S} \times 10^{-2}$ $\left[\frac{g.LA}{g.Glucose}\right]$	q_{LA} $\left[\frac{g}{g.h}\right]$	
			Batch phase	Fed-batch phase			Batch phase	Fed-batch phase			Batch phase	Fed-batch phase
0.05	3.66 ± 0.14[a]	11.0 ± 3.2[b]	0.38 ± 0.014	0.062 ± 0.017	3.57 ± 0.21[a]	10.2 ± 2.5[b]	0.29 ± 0.08	0.022 ± 0.014	20.21 ± 1.15 [a]	55.3 ± 6.2[b]	1.37 ± 0.34	0.2 ± 0.07
0.1	4.49 ± 0.15[a]	14.6 ± 3.6[b]	0.39 ± 0.018	0.066 ± 0.018	3.80 ± 0.24[a]	11.3 ± 1.9[b]	0.34 ± 0.07	0.024 ± 0.017	29.93 ± 0.92[a]	56.8 ± 4.3[b]	1.18 ± 0.25	0.32 ± 0.13
0.15	4.60 ± 0.12[a]	10.2 ± 2.6[b]	0.33 ± 0.012	0.11 ± 0.013	4.73 ± 0.19[a]	12.3 ± 2.6[b]	0.24 ± 0.04	0.051 ± 0.022	31.51 ± 0.83[a]	52.3 ± 3.6[b]	1.67 ± 0.46	0.64 ± 0.15

Estimated values were true and consistent within 95% confidence interval ($p < 0.05$)
[a] Final concentrations of biomass, HA and LA at the end of fed-batch phase
[b]Yield coefficient values were computed at the end of batch phase

Table 4 Final titers, yield coefficients, growth and formation rates of biomass, HA and LA were tabulated during distinct batch and fed-batch phases of the FB control runs carried out at different μ_{SP}

Batch run	Biomass conc. (g/L)	$Y_{X/S} \times 10^{-2}$ $\left[\frac{g.Biomass}{g.Glucose}\right]$	$\mu_{offline}$, (h^{-1})		HA conc. (g/L)	$Y_{HA/S} \times 10^{-2}$ $\left[\frac{g.HA}{g.Glucose}\right]$	q_{HA} $\left[\frac{g}{g.h}\right]$		LA conc. (g/L)	$Y_{LA/S} \times 10^{-2}$ $\left[\frac{g.LA}{g.Glucose}\right]$	q_{LA} $\left[\frac{g}{g.h}\right]$	
			Batch phase	Fed-batch phase			Batch phase	Fed-batch phase			Batch phase	Fed-batch phase
0.05	4.72 ± 0.18[a]	12.2 ± 2.5	0.32 ± 0.017	0.056 ± 0.019	4.22 ± 0.23[a]	08.5 ± 2.2	0.18 ± 0.04	0.083 ± 0.023	18.79 ± 0.93[a]	41.5 ± 4.6	0.91 ± 0.21	0.33 ± 0.12
0.1	6.17 ± 0.21[a]	16.0 ± 1.8	0.33 ± 0.022	0.081 ± 0.024	3.42 ± 0.23[a]	7.1 ± 1.6	0.15 ± 0.07	0.058 ± 0.021	23.22 ± 0.91[a]	55.8 ± 3.9	1.02 ± 0.16	0.43 ± 0.21
0.15	5.14 ± 0.19[a]	12.5 ± 2.8	0.41 ± 0.020	0.095 ± 0.026	3.15 ± 0.21[a]	7.2 ± 1.9	0.14 ± 0.04	0.061 ± 0.032	26.74 ± 0.54[a]	57.1 ± 5.4	0.93 ± 0.26	0.63 ± 0.25

Estimated values were true and consistent within 95% confidence interval ($p < 0.05$)
[a] Final concentrations of biomass, HA and LA at the end of fed-batch phase
[b] Yield coefficient values were computed at the end of batch phase

Figure Legends

Figure 1 Schematic representation of μ_{est} model, its application in feedforward and feedback control strategies

Figure 2 Heat rate (Black continuous) and CER (Pink continuous) profiles showing *S. zooepidemicus* growth, compared with offline biomass growth (Filled circles) depicting batch and fed-batch phases governed by feedforward (FF) approach for different μ_{SP} runs say A. $\mu_{SP} = 0.05\ \mathrm{h}^{-1}$; B. $\mu_{SP} = 0.1\ \mathrm{h}^{-1}$; C. $\mu_{SP} = 0.15\ \mathrm{h}^{-1}$

Figure 3 Heat rate (Black continuous) and CER (Pink continuous) profiles showing *S. zooepidemicus* growth, compared with offline biomass growth (Filled circles) depicting batch and fed-batch phases governed by feedback (FB) approach for different μ_{SP} runs say A. $\mu_{SP} = 0.05\ \mathrm{h}^{-1}$; B. $\mu_{SP} = 0.1\mathrm{h}^{-1}$; C. $\mu_{SP} = 0.15\ \mathrm{h}^{-1}$

Figure 4 Specific growth rates evaluated from the μ_{est} (Black continuous) modeled from calorimetric signal and compared with the measured $\mu_{offline}$ (Filled circles) values for setpoints (Black straight line) A. $\mu_{SP} = 0.05\ \mathrm{h}^{-1}$; B. $\mu_{SP} = 0.1\ \mathrm{h}^{-1}$; C. $\mu_{SP} = 0.15\ \mathrm{h}^{-1}$ in a feedforward (FF) strategy.

Figure 5 Specific growth rates evaluated from the μ_{est} (Black continuous) modeled from calorimetric signal and compared with the measured $\mu_{offline}$ (Filled circles) values for setpoints

(Black straight line) A. $\mu_{SP} = 0.05\ \mathrm{h}^{-1}$; B. $\mu_{SP} = 0.1\ \mathrm{h}^{-1}$; C. $\mu_{SP} = 0.15\ \mathrm{h}^{-1}$ in a feedback (FB) strategy.

Figure 6 Dynamic plot representing the estimated titers of DCW (Red circles), HA (Blue circles), LA (Brown circles), Glucose values (Green circles) and feed rate (mL/h) (Black continuous) was carried out during feed forward (FF) control strategy for μ_{SP}. A. $\mu_{SP} = 0.05\ \mathrm{h}^{-1}$; B. $\mu_{SP} = 0.1\ \mathrm{h}^{-1}$; C. $\mu_{SP} = 0.15\ \mathrm{h}^{-1}$.

Figure 7 Dynamic plot representing the estimated titers of DCW (Red circles), HA (Blue circles), LA (Brown circles), Glucose values (Green circles) and feed rate (mL/h) (Black continuous) was carried out during feedback (FB) control strategy for μ_{SP}. A. $\mu_{SP} = 0.05\ \mathrm{h}^{-1}$; B. $\mu_{SP} = 0.1\ \mathrm{h}^{-1}$; C. $\mu_{SP} = 0.15\ \mathrm{h}^{-1}$.

Figure 8 Final DCW, HA and LA concentrations estimated at the completion of fed-batch fermentation employing A. Feed forward (FF) strategy and B. Feed back (FB) strategy

Figure 9 Molecular weight and Polydispersity index computed during fed batch runs (A. Feedforward (FF) and B. Feedback (FB) control strategies operated at different μ_{SP}.

References

1. Kushboo G, Krishna MP. Mechanistic and therapeutic overview of glycosaminogylcans: the unsung heroes of biomolecular signaling. Glycoconj J. 2016;33:1-17
2. Park YB, Ha CW, Lee CH, Yoon YC, Park YG. Cartilage Regeneration in Osteoarthritic Patients by a Composite of Allogeneic Umbilical Cord Blood-Derived Mesenchymal Stem Cells and Hyaluronate Hydrogel: Results from a Clinical Trial for Safety and Proof-of Concept with 7 Years of Extended Follow-Up. Stem Cells Transl Med. 2016;6:613-621.
3. Gloria H, Kristina N, Gabriela A, Lukas K, Vladimir V. An Effective Translation: The Development of Hyaluronan-Based Medical Products from the Physiochemical and Preclinical Aspects. Front BioengBiotechnol. 2018:6(62).
4. Andre P. Hyaluronic acid and its use as “rejuvenation” agent in cosmetic dermatology. Semin Cutan Med Surg. 2004:23(4):218-222
5. Göllner I, Voss W, von Hehn U, Kammerer S. Ingestion of an Oral Hyaluronan Solution Improves Skin Hydration, Wrinkle Reduction, Elasticity and Skin Roughness: Results of Clinical Study. J Evid-Based Integr Med. 2017;22(4):816-823.
6. J.E. Rayahin, J.S. Buhrman, Y. Zhang, T.J. Koh, R.A. Gemeinhart. High and Low Molecular Weight Hyaluronic Acid Differentially Influence Macrophage Activation. ACS Biomater. Sci. Eng. 1 (2015) 481 - 493.
7. J.H. Im, J.M. Song, J.H. Kang, D.J. Kang, Optimization of medium components for high-molecular-weight hyaluronic acid production by *Streptococcus sp.* ID9102 via a statistical approach. Journal of Industrial Microbiology and Biotechnology 36 (2009) 1337 – 1344.

8. Karl M, John WP. The Polysaccharide of Vitreous Humor. J Biol Chem. 1934;107:629-634
9. Park YB, Ha CW, Lee CH, Yoon YC, Park YG. Cartilage Regeneration in Osteoarthritic Patients by a Composite of Allogeneic Umbilical Cord Blood-Derived Mesenchymal Stem Cells and Hyaluronate Hydrogel: Results from a Clinical Trial for Safety and Proof-of Concept with 7 Years of Extended Follow-Up. Stem Cells Transl Med. 2016;6:613-621.
10. Pierre AMD. New trends in face rejuvenation by hyaluronic acid injections. J Cosmet Dermatol. 2008;7(4):251-258.
11. Shin K, Yoshiyuki F, Norie A, Keiko K, Masako A, Takaya N, Kumiko G, Takeshi I, Sei S, Shinichi O, Shogo O, Osamu N, Hideyuki S, Kanji S. Inflammatory mediator ultra-low-molecular-weight hyaluronan triggers necrosis of B-precursor leukemia cells with high surface CD44 expression. Cell Death Dis. 2017; 8:e2857.
12. Shayne S, Norman FT, Tatina S. Encapsulation of PEGylated low-molecular-weight PEI polyplexes in hyaluronic acid hydrogels reduces aggregation. Acta Biomater. 2015;28:45-54.
13. Carmen GB, Jan S, Floor KK, Lambertus AMB, Gerrit E. Production methods for Hyaluronan. Int J Carbohydr Chem. 2013;624967.
14. Naresh M, Satya SP, Akshay A, Nivedhitha S, Senthilkumar S. Calorespriometric investigation of *Streptococcus zooepidemicus* metabolism: Thermodynamics of anabolic payload contribution by growth and hyaluronic acid synthesis. BiochemEng J. 2019;152,107367.

15. Naoki I, Masaki S, Toshiro S, Takeshi O, Hisao O. Hyaluronic acid production by recombinant *Streptococcus thermophilus*. J BiosciBioeng. 2011;111:665-670.
16. Lars MB, Philip H, Lars KN. Evolution of the Hyaluronic Acid Synthesis (has) Operon in *Streptococcus zooepidemicus* and Other Pathogenic *Streptococci.* J Mol Evol. 2008;67:13-22.
17. DeAngelis PL, Jing W, Drake RR, Achyuthan AM. Identification and Molecular Cloning of a Unique Hyaluronan Synthase from *Pasteurella multocida*. J Biol Chem. 1998;273:8454-8458.
18. Widner B, Behr R, von Dollen S, Tang M, Heu T, Sloma A, Sternberg D, DeAngelis PL, Weigel PH, Brown S. Hyaluronic Acid Production in *Bacillus subtilis*. Appl Environ Microbiol 2005;71:3747-3752.
19. Huimin Y, Stephanopoulos G. Metabolic engineering of *Escherichia coli* for biosynthesis of hyaluronic acid. Metab Eng. 2008;10:24-32.
20. Euijoon J, Woo YS, Jung HK. Metabolic engineering of *Pichia pastoris* for production of hyaluronic acid with high molecular weight. J Biotechnol. 2014;185, 28 – 36.
21. Prasad SB, Jayaraman G, Ramachandran KB. Hyaluronic acid production is enhanced by the additional co-expression of UDP-glucose pyrophosphorylase in *Lactococcus lactis*. Appl Microbiol Biotechnol. 2010;86:273-283.
22. Cheng F, Luozhang S, Guo Z, Yu H, Stephanopoulus G. Enhanced Biosynthesis of Hyaluronic Acid Using Engineered *Corynebacterium glutamicum* Via Metabolic Pathway Regulation. Biotechnol J. 2017;12:1700191.
23. Mao Z, Chen RR. Recombinant synthesis of Hyaluronan by *Agrobacterium sp.* Biotechnol Prog. 2007;23:1038-1042.

24. Armstrong DC, Johns MR. Culture Conditions Affect the Molecular Weight Properties of Hyaluronic Acid Produced by *Streptococcus zooepidemicus*. Appl Environ Microbiol. 1997;63:2759-64.

25. Swaminathan J, Ramachandran KB. Influence of competing metabolic processes on the molecular weight of hyaluronic acid synthesized by *Streptococcus zooepidemicus*. BiochemEng J. 2010;48:148-158.

26. Sneh SB, Guhan J, Ramachandran KB. Ratio of intracellular precursors concentrations and their flux influences hyaluronic acid molecular weight in *Streptococcus zooepidemicus* and recombinant *Lactococcus lactis*. Bioresour Technol 2014; 163: 222-227.

27. Minsung C, Saeed MAZ, Sang YL. Kinetic model-based feed-forward controlled fed-batch fermentation of *Lactobacillus rhamnosus* for the production of lactic acid from Arabic date juice. Bioprocess Biosyst Eng. 2014;37:1007-1015.

28. Oliver S, Denes Z, Christian D, Christoph H. Quantitative comparison of dynamic physiological feeding profiles for recombinant protein production with *Pichia pastoris*. Bioprocess Biosyst Eng. 2014;37:1163-1172.

29. Carl FM, Robert G. Mini-review: soft sensors as means for PAT in the manufacture of bio-therapeutics. J Chem Technol Biotechnol. 2015;90:215-227

30. Naresh M, Senthilkumar S. Heat Compensation Calorimeter as a Process Analytical Tool to Monitor and Control Bioprocess Systems. Ind Eng Chem Res. 2017;56:8416 – 8427.

31. Biener R, Steinkämper A, Hofmann J. Calorimetric control for high cell density cultivation of a recombinant *Escherichia coli* strain. J Biotechnol. 2010;146:45-53.

32. Biener R, Steinkämper A, Horn T. Calorimetric control of the specific growth rate during fed-batch cultures of *Saccharomyces cerevisiae*. J Biotechnol. 2012;160:195-201.

33. Sivaprakasam S, Schuler MM, Hama A, Hughes KM, Marison IW. Biocalorimetry as a Process analytical technology process analyzer; robust in-line monitoring and control of aerobic fed-batch cultures of crabtree-negative yeast cells. J Therm Anal Calorim. 2011;104(1), 75-85.

34. Hansen, L. D., Macfarlane, C., McKinnon, N., Smith, B. N., & Criddle, R. S. Use of calorespirometric ratios, heat per CO_2 and heat per O_2, to quantify metabolic paths and energetics of growing cells. Thermochimica Acta. 2004; 422(1-2), 55-61.

35. Skolik, R. A., Konkle, M. E., & Menze, M. A. Calorespirometry: A Powerful, Noninvasive Approach to Investigate Cellular Energy Metabolism. Journal of Visualized Experiments. 2018; (135), e57724.

36. Matheson, S., Ellingson, D. J., McCarlie, V. W., Smith, B. N., Criddle, R. S., Rodier, L., & Hansen, L. D. Determination of growth and maintenance coefficients by calorespirometry. Functional plant biology. 2004; 31(9), 929-939.

37. Naresh M, Subbi RRT, Satya SP, Senthilkumar S. Deciphering the role of dissolved oxygen and N-acetyl glucosamine in governing high molecular weight hyaluronic acid synthesis in *Streptococcus zooepidemicus* factory. Appl Microbiol Biotechnol. 2020;104:3349-3360

38. Gary LK, Jeffery JC, Gregory WL, William RS. A Predictive and Feedback Control Algorithm Maintains a Constant Glucose Concentration in Fed-Batch Fermentations. Appl Environ Microbiol. 1991;57(4):910-917

39. Mandeep K, Guhan J. Hyaluronan production and molecular weight is enhanced in pathway-engineered strains of lactate dehydrogenase-deficient *Lactococcus lactis*. MetabEngCommun. 2016;3:15-23

40. Srikanth K, Naresh M, Satya SP, Uttariya P, Senthilkumar S. Control of specific growth rate for the enhanced production of human interferon α2b in glycoengineered *Pichia pastoris*: process analytical technology guided approach. J Chem Technol Biotechnol. 2019;94(10):3111-3123

41. Michal D, Moira MS, Ian WM. Simple control of specific growth rate in biotechnological fed-batch processes based on enhanced online measurements of biomass. Bioprocess Biosyst Eng. 2010; 33(9):1109-1118.

42. Nadia O, Pierrick L, Christelle HS, Emmanuel R, Stėphane M, Roman K, Ivan M. CTAB turbidimetric method for assaying hyaluronic acid in complex environments and under cross-linked form. Carbohydr Polym. 2014;112(4), 102-108.

43. Moria MS, Senthilkumar S, Brian F, Adel H, Katie MH, Ian WM. Investigation of the potential of biocalorimetry as a process analytical technology (PAT) tool for monitoring and control of Crabtree-negative yeast cultures. Appl Microbiol Biotechnol. 2012;93:575-584

44. Patrick W, Patrick S, Christoph H. Real-time estimation of biomass and specific growth rate in in physiologically variable recombinant fed-batch processes. Bioprocess Biosyst Eng. 2013;36:1205-1218.

Nomenclature

Abbreviations:

CD44 Cluster of Differentiation 44

CH Compensation Heater

CTAB Cetyltrimethyl-Ammmonium bromide

DAQ Data Acquisition

FB Feedback

FF Feedforward

HA Hyaluronic acid

PAT Process Analytical Technology

PID Proportional, Integrative and Derivative Control

SDS Sodium Dodecyl Sulphate

Variables and Constants:

$q_{Baseline}$ Baseline heat rate [W/L]

q_C Compensation heat rate [23 W]

q_B Biological heat rate [W/L]

q_S Agitation heat rate [W/L]

q_A Aeration heat loss [W/L]

q_E Environmental heat loss [W/L]

q_J Heat flow from reaction broth to jacket [W/L]

T_r Reactor temperature [K]

$Y_{Q/X}$ Heat yield due to Biomass formation

Greek symbol:

μ Specific growth rate

τ Integral time

Acknowledgement

Authors are more pleased to convey thanks to Prof. Guhan Jayaraman (IIT Madras) for his technical inputs. Mr. Sanjeeva kumar, Graduate student is kindly acknowledged for his support in carrying out reactor operations. Authors also owe much grateful to Dept. of Biosciences and Bioengineering, IIT Guwahati for providing state of art analytical instruments for the successful completion of this work.

Author's contribution and consent

All authors significantly contributed to the successful execution of this work. NM and SSP were instrumental in devising the process control strategy and carried out experimental reactor runs. SS* conceptually mentored the design of soft sensor based monitoring and control of the bioprocess, also supervised the entire work. AJ and SR analyzed the experimental samples for the estimation of specific growth rate and analyte concentrations. The manuscript drafting was jointly contributed and peer reviewed by NM, SSP and SS*. Consent from all the authors have been obtained before the submission. All the authors carefully reviewed the manuscript before its

submission and approve the authority of the entire work deemed to be the discretion of corresponding author (SS*).

Data and material availability

All the data and illustrations produced in the article can be made available for academic research and teaching upon approval by corresponding author and editor.

Funding Acknowledgement

Authors sincerely acknowledge Department of Biotechnology (Govt. of India) for the generous funding in proceeding with our research objectives (No. BT/PR5789/PID/6/680/2012) and would like to thank Ministry of Education (MoE, Govt. of India) for funding the manpower.

Ethics approval and statement

No animal/specimen/organ from animal source was used in this study. Approval of ethical committee is not applicable for this work.

Conflict of interest

All Authors declare that they have no conflict of interest.

Figures

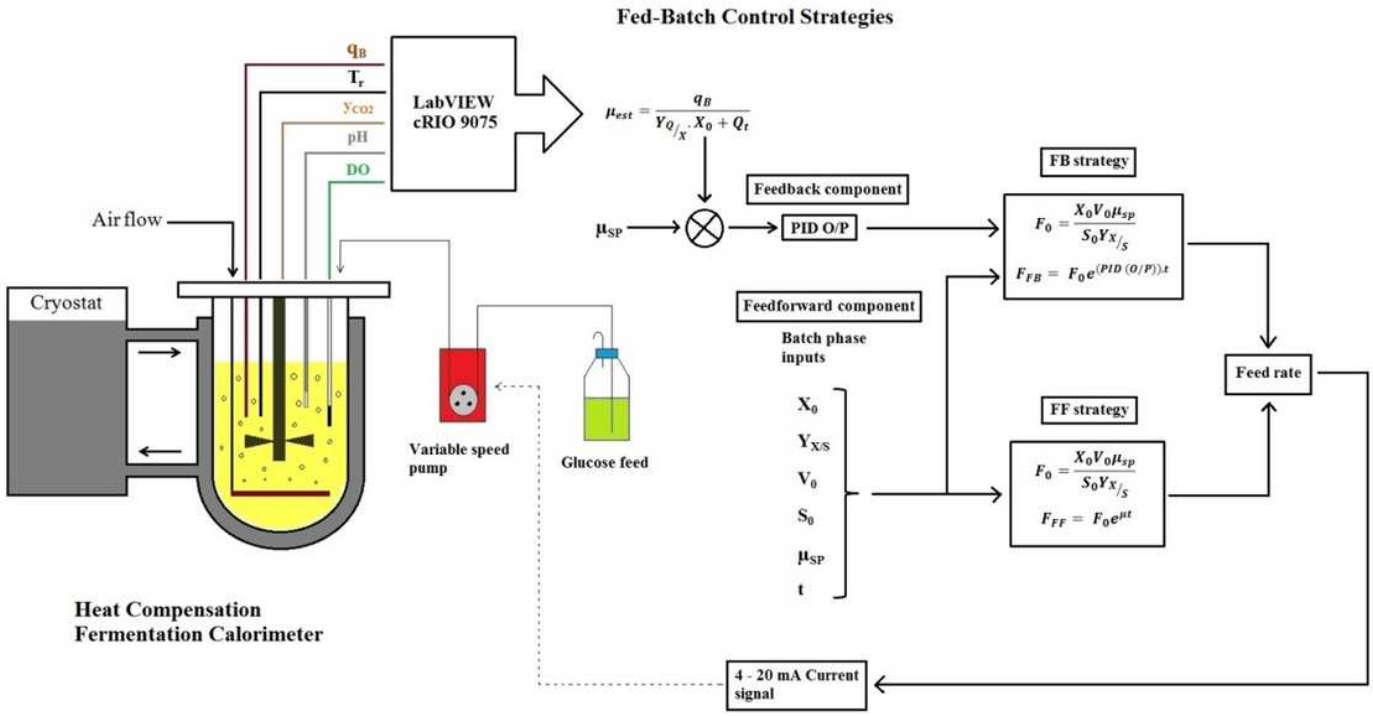

Figure 1

Schematic representation of μest model, its application in feedforward and feedback control strategies

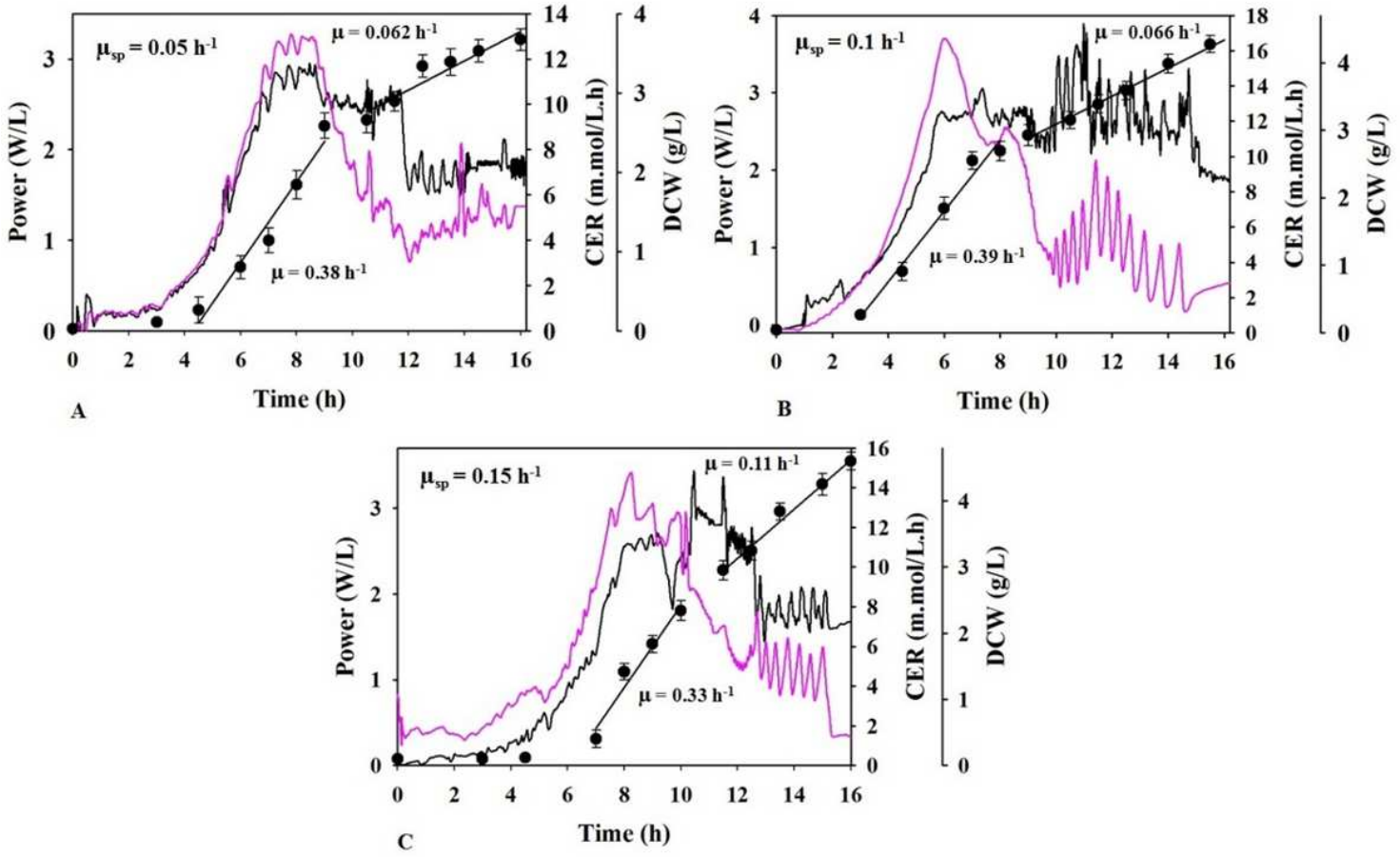

Figure 2

Heat rate (Black continuous) and CER (Pink continuous) profiles showing S. zooepidemicus growth, compared with offline biomass growth (Filled circles) depicting batch and fed-batch phases governed by feedforward (FF) approach for different μ_SP runs say A. μ_SP=0.05 h^(-1); B. μ_SP=0.1 h^(-1); C. μ_SP=0.15 h^(-1)

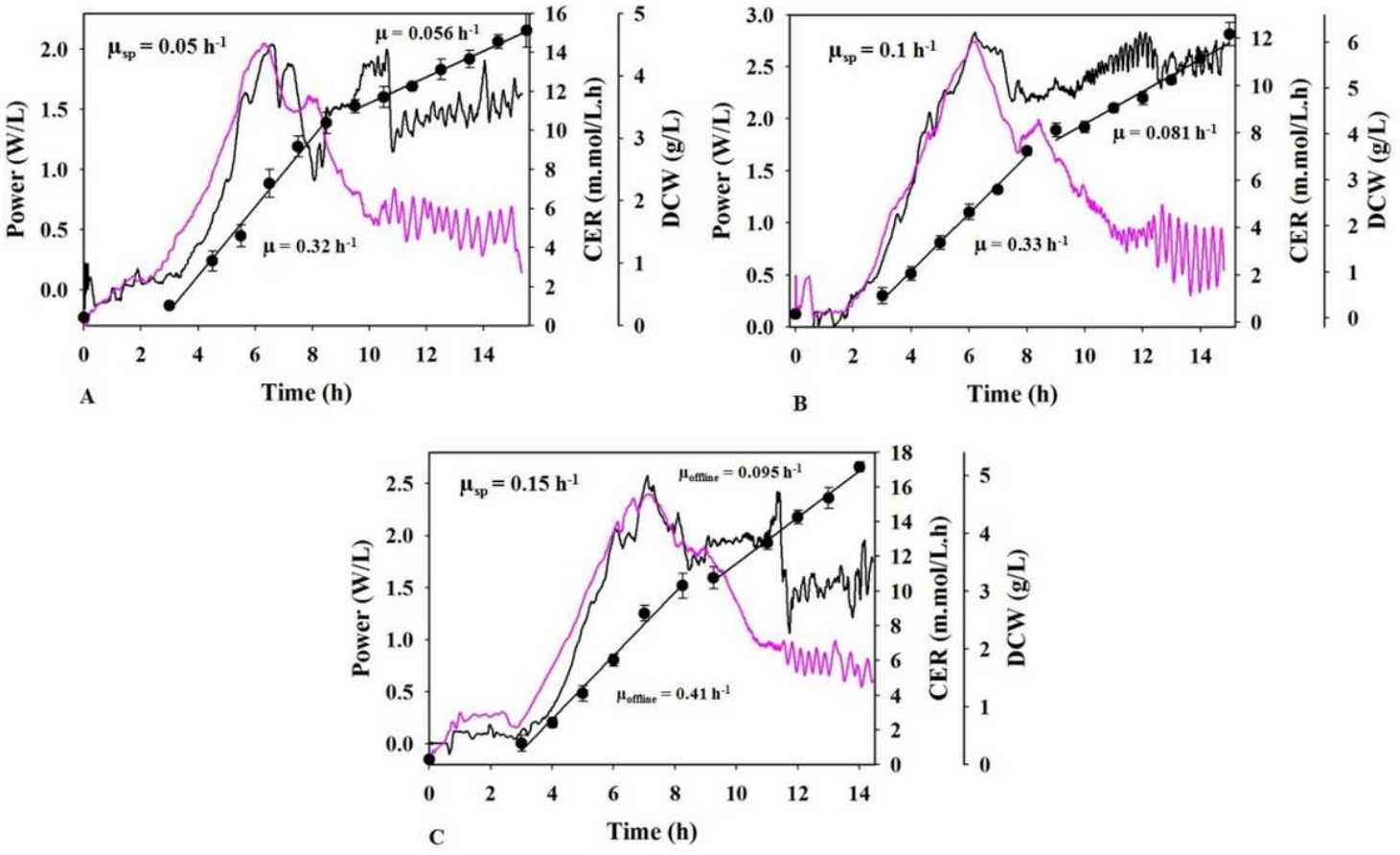

Figure 3

Heat rate (Black continuous) and CER (Pink continuous) profiles showing S. zooepidemicus growth, compared with offline biomass growth (Filled circles) depicting batch and fed-batch phases governed by feedback (FB) approach for different μ_SP runs say A. μ_SP=0.05 h^(-1); B. μ_SP=0.1h^(-1); C. μ_SP=0.15 h^(-1)

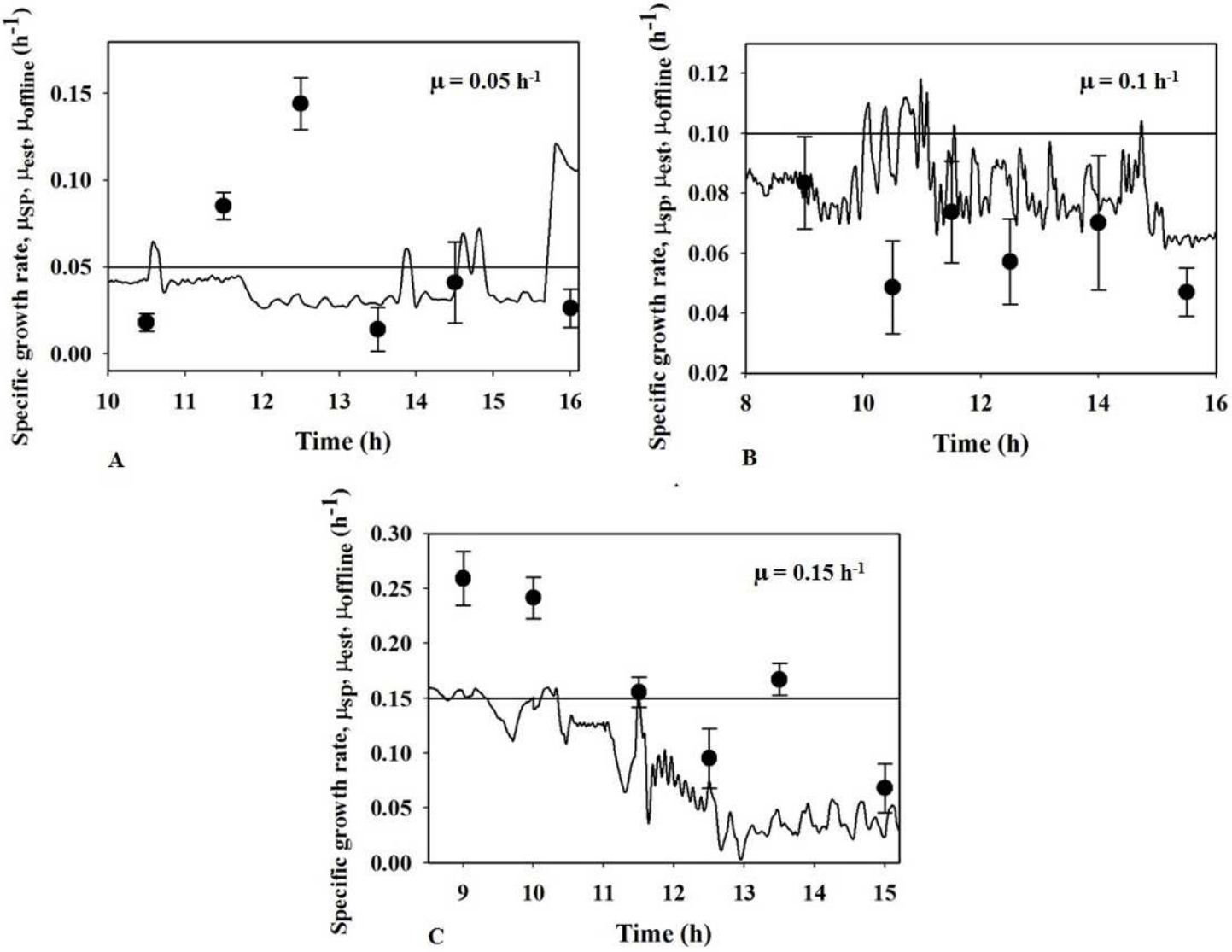

Figure 4

Specific growth rates evaluated from the μ_est (Black continuous) modeled from calorimetric signal and compared with the measured μ_offline (Filled circles) values for setpoints (Black straight line) A. μ_SP=0.05 h^(-1); B. μ_SP=0.1 h^(-1); C. μ_SP=0.15 h^(-1) in a feedforward (FF) strategy.

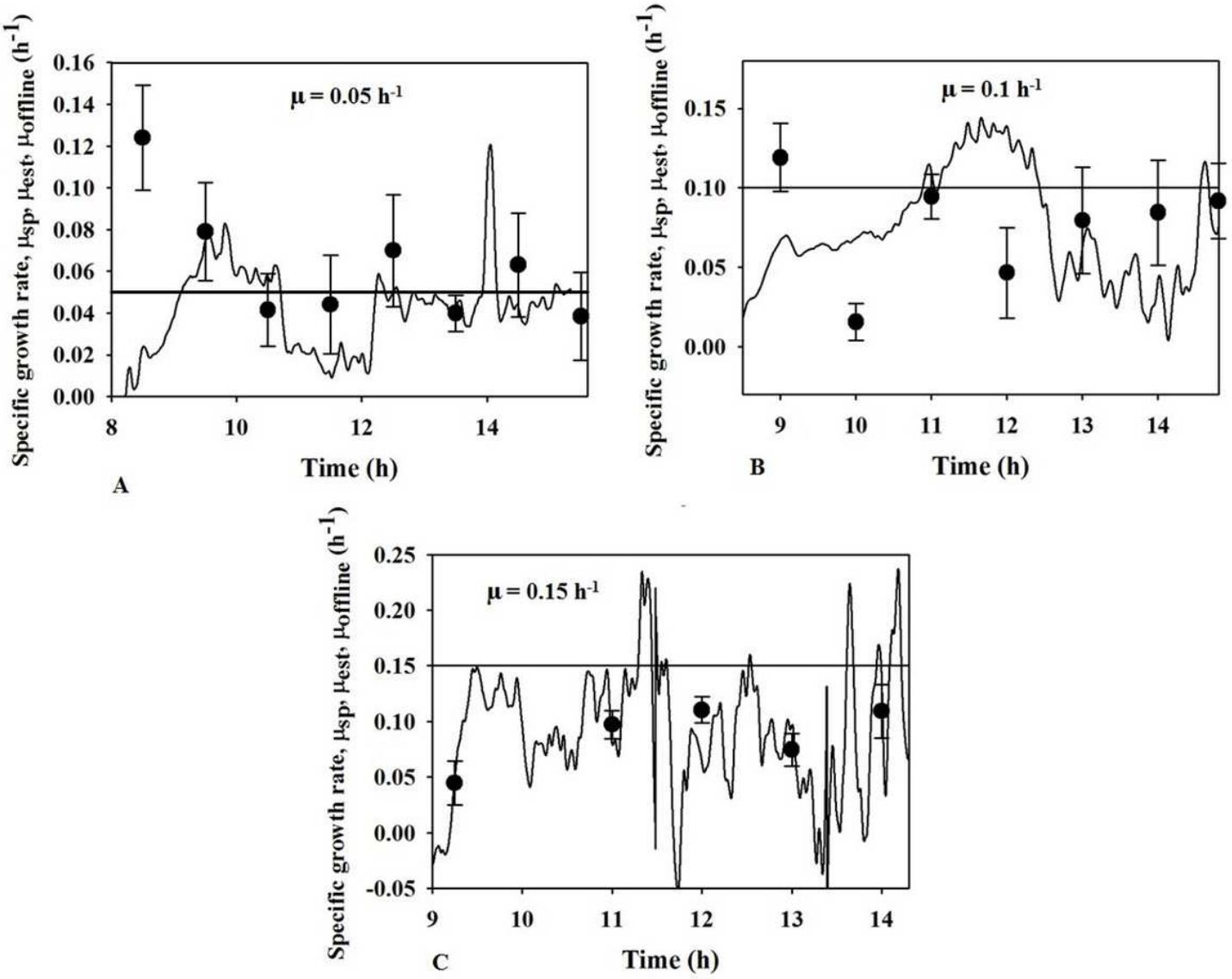

Figure 5

Specific growth rates evaluated from the μ_est (Black continuous) modeled from calorimetric signal and compared with the measured μ_offline (Filled circles) values for setpoints (Black straight line) A. μ_SP=0.05 h^(-1); B. μ_SP=0.1 h^(-1); C. μ_SP=0.15 h^(-1) in a feedback (FB) strategy.

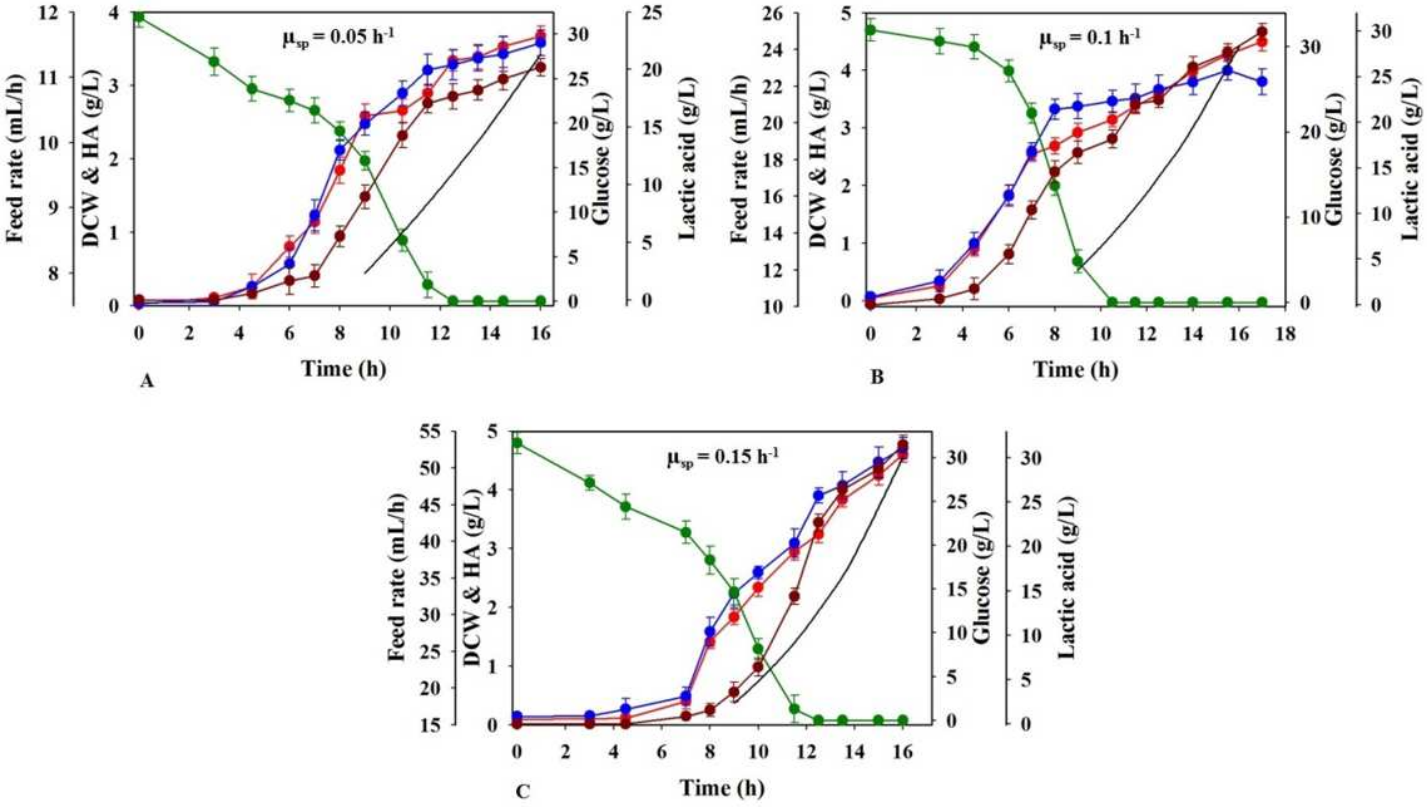

Figure 6

Dynamic plot representing the estimated titers of DCW (Red circles), HA (Blue circles), LA (Brown circles), Glucose values (Green circles) and feed rate (mL/h) (Black continuous) was carried out during feed forward (FF) control strategy for μ_SP. A. μ_SP=0.05 h^(-1); B. μ_SP=0.1 h^(-1); C. μ_SP=0.15 h^(-1).

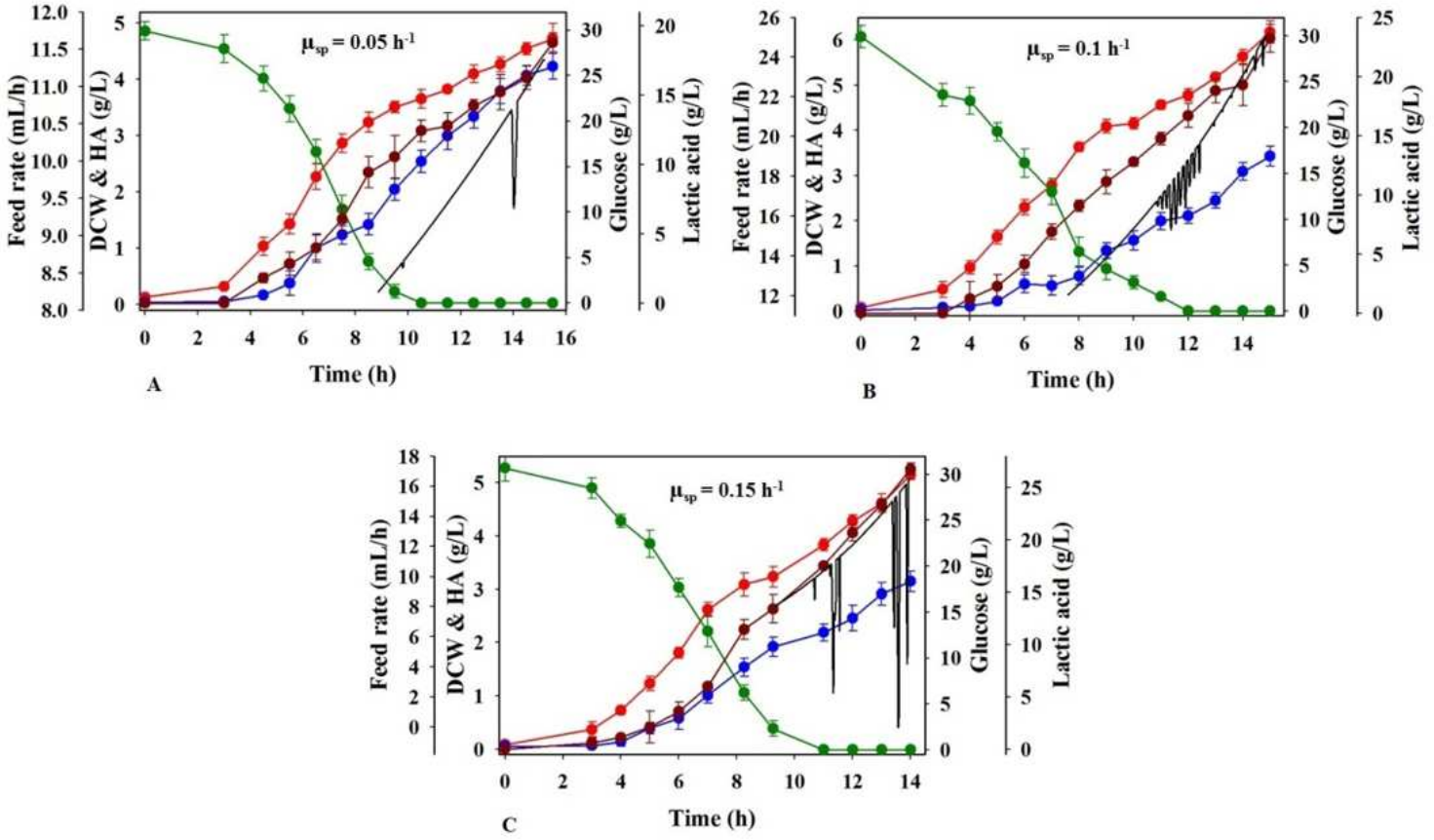

Figure 7

Dynamic plot representing the estimated titers of DCW (Red circles), HA (Blue circles), LA (Brown circles), Glucose values (Green circles) and feed rate (mL/h) (Black continuous) was carried out during feedback (FB) control strategy for μ_SP. A. μ_SP=0.05 h^(-1); B. μ_SP=0.1 h^(-1); C. μ_SP=0.15 h^(-1).

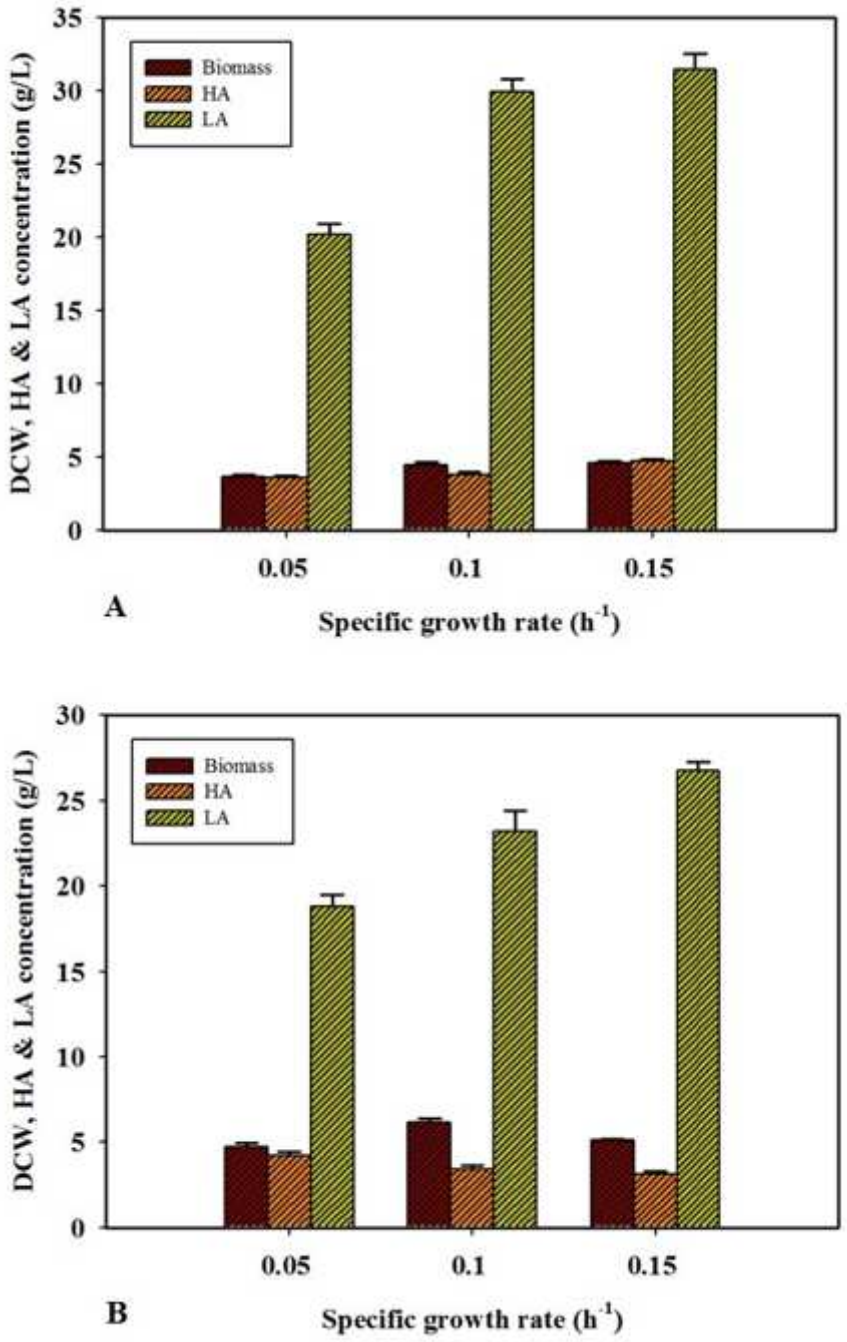

Figure 8

Final DCW, HA and LA concentrations estimated at the completion of fed-batch fermentation employing A. Feed forward (FF) strategy and B. Feed back (FB) strategy

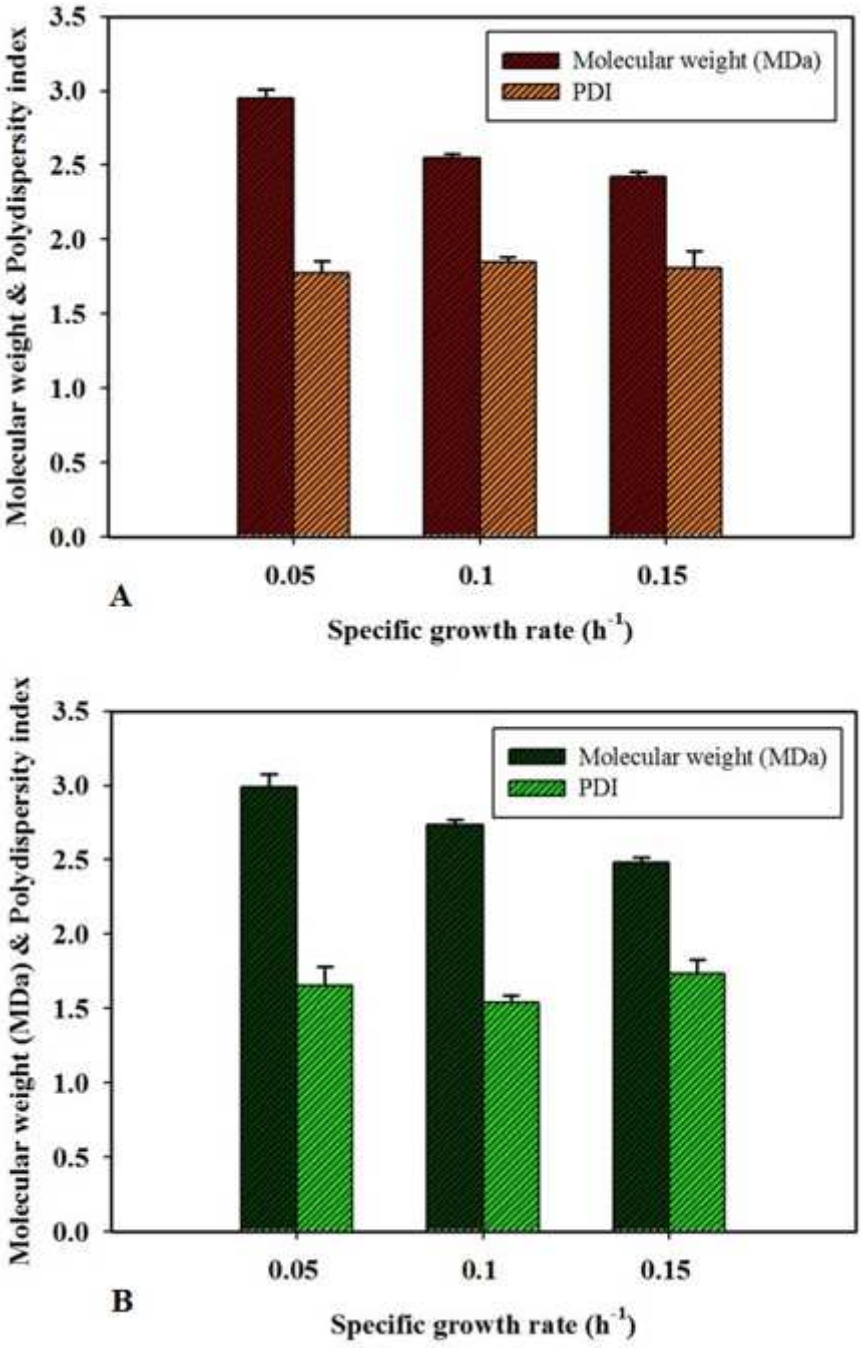

Figure 9

Molecular weight and Polydispersity index computed during fed batch runs (A. Feedforward (FF) and B. Feedback (FB) control strategies operated at different μ_SP.

Supplementary Files

This is a list of supplementary files associated with this preprint. Click to download.

- SupplementaryInformation.docx

- Annexurel.docx